HHS Public Access

Author manuscript

Nat Immunol. Author manuscript; available in PMC 2014 April 01.

Published in final edited form as:

Nat Immunol. 2013 October ; 14(10): 1073–1083. doi:10.1038/ni.2707.

Differential regulation of lymphopoiesis and leukemogenesis by individual zinc fingers of Ikaros

Hilde Schjerven[1,2,8], **Jami McLaughlin**[1], **Teresita L. Arenzana**[1,2], **Seth Frietze**[7,8], **Donghui Cheng**[1,3], **Sarah Wadsworth**[1,2], **Gregory W. Lawson**[5,6], **Steven J. Bensinger**[2,6], **Peggy J. Farnham**[7], **Owen N. Witte**[1,2,3,4], and **Stephen T. Smale**[1,2,4]

[1]Department of Microbiology, Immunology, and Molecular Genetics, University of California, Los Angeles, CA 90095, USA

[2]Molecular Biology Institute, University of California, Los Angeles, CA 90095, USA

[3]Howard Hughes Medical Institute, University of California, Los Angeles, CA 90095, USA

[4]Eli and Edythe Broad Center of Regenerative Medicine and Stem Cell Research, University of California, Los Angeles, CA 90095, USA

[5]Division of Laboratory Animal Medicine, University of California, Los Angeles, CA 90095, USA

[6]Department of Pathology and Laboratory Medicine, University of California, Los Angeles, CA 90095, USA

[7]Department of Biochemistry and Molecular Biology, USC/Norris Comprehensive Cancer Center, University of Southern California, Los Angeles, CA 90089, USA

Abstract

C2H2 zinc fingers are found in several transcriptional regulators in the immune system. However, these proteins usually contain more fingers than are needed for stable DNA binding, suggesting that different fingers regulate different genes and functions. Mice lacking finger 1 or finger 4 of Ikaros exhibited distinct subsets of the phenotypes of Ikaros-null mice. Most notably, the two fingers controlled different stages of lymphopoiesis and finger 4 was selectively required for tumor suppression. The distinct phenotypes suggest that only a small number of Ikaros target genes are critical for each of its biological functions. Subdivision of phenotypes and targets by mutagenesis of individual fingers will facilitate efforts to understand how members of this prevalent family regulate development, immunity and disease.

Correspondence should be addressed to S.T.S. (smale@mednet.ucla.edu).

[8]Present addresses: Department of Laboratory Medicine, University of California, San Francisco, CA 94143, USA (H.S.) and School of Biological Sciences, University of Northern Colorado, Greeley, CO 80639, USA (S.F.)

Accession codes. GEO: RNA-Seq and ChIP-Seq data, GSE33693.

Note: Supplementary information is available on the Nature Immunology website.

Author Contributions: H.S., J.M., T.L.A., S.F., D.C., S.W., and G.W.L. designed and performed experiments, and analyzed data; S.J.B. provided intellectual input and experimental advice; P.J.F., O.N.W. and S.T.S. supervised research and analyzed data. H.S. and S.T.S wrote the manuscript.

Competing Financial Interests: The authors declare no competing financial interests.

In the post-genomics era, a critical goal is to define the target genes and mechanisms of action of transcription factors that contribute to development, disease and the response to environmental cues. Although progress has been rapid, a major hurdle is that many factors are involved in several biological pathways and can contribute to multiple steps in a single pathway, making it difficult to study key regulatory events in isolation.

Ikaros is one transcription factor that regulates numerous biological events. Ikaros-null (*Ikzf1*^{null}) mice lack B lineage cells, natural killer (NK) cells, peripheral lymph nodes and fetal T cells, and they exhibit a number of other abnormalities[1-3]. Adult B cells are absent due to an inability of lymphoid-primed multipotent progenitors (LMPPs) to develop into common lymphoid progenitors (CLPs)[4], but Ikaros also regulates later stages of B cell development[5-9]. Moreover, mice containing mutations in the Ikaros-encoding *Ikzf1* gene develop thymic lymphoma with high penetrance[10,11].

In humans, mutations at the *IKZF1* locus have been observed in a high percentage of BCR-ABL^{+} B-ALL and high-risk B cell-progenitor ALL samples[12,13]. *IKZF1* was the only gene for which mutations were found to predict a poor response to therapy[13], yet the mechanisms responsible for tumor suppression by Ikaros remain poorly understood. Ikaros is thought to contribute to both the activation and repression of transcription, with the Mi-2/NuRD complex as a predominant interacting partner[14-16]. Importantly, the target genes responsible for most of the key phenotypes of *Ikzf1* mutant mice remain unknown[7,17-19]. The widespread deregulation of gene expression in *Ikzf1* mutant cells and the finding that Ikaros binds several thousand genomic sites have increased the challenge of uncovering the mechanisms by which Ikaros regulates development and leukemogenesis[16,20].

Members of the Ikaros family contain a conserved DNA-binding domain near the N-terminus, usually with four C2H2 zinc fingers[21]. Ikaros family members also contain two C-terminal C2H2 zinc fingers dedicated to dimerization and multimerization[22-24]. C2H2 zinc fingers are found in many ubiquitous transcription factors and in numerous proteins involved in tissue-specific and developmental stage-specific transcription[25-27], including the PLZF, Bcl-6, Gfi1, Blimp1, and ThPOK proteins in the immune system.

Stable DNA binding *in vitro* by a C2H2 zinc finger protein usually requires two or three tandem fingers[27,28]. In Ikaros, fingers 2 and 3 are sufficient for stable binding and recognize the core consensus sequence, GGGAA. In contrast, fingers 1 and 4 appear to modulate binding to specific sites[29-31]. In addition to full-length Ikaros (Ik-1), most or all hematopoietic cells abundantly express a smaller isoform that lacks finger 1 (Ik-2). Ikaros isoforms lacking other fingers due to alternative pre-mRNA splicing have been observed, but these isoforms are generally much less abundant except in transformed cell lines[29,32,33].

Given that two or three fingers are generally sufficient for stable DNA binding[28], it is striking that most zinc finger DNA-binding proteins contain more than three tandem fingers. The reasons for this phenomenon have been of interest since the early studies of the nine-finger TFIIIA protein[27,34,35]. All of the tandem fingers may be required for stable binding to key targets *in vivo*, with the multiple fingers recognizing extended DNA regions with high specificity. Alternatively, defined subsets of fingers may recognize distinct target genes.

Initial support for the latter hypothesis emerged from *in vitro* protein-DNA interaction studies showing that different combinations of fingers from TFIIIA, Ikaros, CTCF and other proteins can bind different DNA sequences[29,30,35-39]. In addition, ChIP-Seq studies of ectopically expressed CTCF mutant proteins have revealed that CTCF binding sites can be separated into distinct classes, due to binding by different finger subsets and possibly leading to different functional outcomes[40].

To determine in a physiological setting whether multi-finger DNA-binding proteins use different fingers to regulate different genes and biological functions, or whether all functions require the full complement of fingers, we generated two new *Ikzf1* mutant mouse strains containing germline deletions of the exons encoding fingers 1 and 4. Phenotypic analyses suggest that the two fingers regulate distinct biological events. Transcriptome profiling confirmed that the two fingers regulate distinct sets of genes, and DNA-binding analyses confirmed that fingers 1 and 4 can modulate binding to different genomic sites. Finally, *in vitro* and *in vivo* models of BCR-ABL$^+$ B-ALL established parallels between tumor suppression in thymocytes and in B-ALL. Together, these results suggest that multi-finger DNA-binding domains exist, at least in part, to allow different fingers to regulate different genes. Moreover, the strikingly different phenotypes of the mutant strains suggest that each developmental step and biological function regulated by Ikaros is dependent on the proper regulation of only a small number of Ikaros target genes.

Results

Generation of mutant mouse strains

Mice lacking Ikaros zinc finger 1 (F1, strain *Ikzf1*$^{\Delta F1/\Delta F1}$) or finger 4 (F4, strain *Ikzf1*$^{\Delta F4/\Delta F4}$) were generated by germline deletion of exon 4 or exon 6, respectively (Supplementary Fig. 1a). Each deletion generated a mutant protein that lacks a zinc finger and a small number of adjacent residues. Exon 4 encodes 87 residues, including the 23 residues of finger 1, 63 residues preceding the finger, and one residue following the finger. Exon 6 encodes only 41 residues. The 24-residue finger 4 is preceded by four residues that comprise the linker between fingers 3 and 4; these residues closely resembles the linker consensus sequence found in most zinc finger proteins[28]. After the finger, exon 6 encodes 13 additional residues; two prolines near the end of this region may separate the DNA-binding domain from an exon 7-encoded domain.

Correct targeting of the *Ikzf1* exons was confirmed by Southern blot, PCR (data not shown) and immunoblot (Fig. 1a). *Ikzf1*$^{\Delta F1/\Delta F1}$ thymocytes lacked the full-length Ikaros isoform, Ik-1, but expressed Ik-2, which in wild-type mice is generated by alternative pre-mRNA splicing[2]. In the *Ikzf1*$^{\Delta F4/\Delta F4}$ strain, deletion of exon 6 reduced the sizes of both Ik-1 and Ik-2 (Fig. 1a). RNA-Seq analysis of thymocyte mRNA further confirmed correct targeting, as reads from exons 4 and 6 were absent in the *Ikzf1*$^{\Delta F1/\Delta F1}$ and *Ikzf1*$^{\Delta F4/\Delta F4}$ samples, respectively (Fig. 1b).

Initial analysis of mutant strains

Examination of the *Ikzf1*$^{\Delta F1/\Delta F1}$ and *Ikzf1*$^{\Delta F4/\Delta F4}$ phenotypes was initiated soon after the mice were generated, but all phenotypes have been confirmed after backcrossing onto a C57BL/6 background through nine or more generations. Efforts to backcross *Ikzf1*^{null} mice have been unsuccessful (K. Georgopoulos and S. Winandy, personal communication), presumably because the null mutation results in embryonic lethality in a C57BL/6 background. The successful backcrossing of the *Ikzf1*$^{\Delta F1/\Delta F1}$ and *Ikzf1*$^{\Delta F4/\Delta F4}$ strains provided initial evidence that neither finger 1 nor finger 4 is required for all functions of Ikaros.

Initial studies revealed that the development of CD11b^{+} myeloid cells is unperturbed in both strains, similar to the phenotype of *Ikzf1*^{null} mice (Fig. 1c and Supplementary Fig. 1b). Conventional B cells were also observed in the bone marrow and spleen of both mutant mice, albeit at reduced levels (Fig. 1d and Supplementary Fig. 1c,d). The presence of B cells contrasts with the absence of all B lineage cells in *Ikzf1*^{null} mice. These results suggest that DNA-binding fingers 2 and 3 are sufficient for a fraction of hematopoietic progenitors to successfully progress through B cell development.

B-cell development phenotypes

A detailed examination of B cell development (Supplementary Fig. 2)[41,42] revealed striking differences between *Ikzf1*$^{\Delta F1/\Delta F1}$, *Ikzf1*$^{\Delta F4/\Delta F4}$ and *Ikzf1*^{null} mice. First, in contrast to the absence of pre-pro-B cells in *Ikzf1*^{null} mice due to a block in LMPP maturation[4], *Ikzf1*$^{\Delta F1/\Delta F1}$ and *Ikzf1*$^{\Delta F4/\Delta F4}$ mice contained relatively normal numbers of these cells. The B220^{+}CD43^{+}CD24^{-}BP-1^{-} population contains NK cell precursors and plasmacytoid dendritic cells (pDCs) in addition to pre-pro-B cells, which when initially analyzed showed a reduction in *Ikzf1*$^{\Delta F4/\Delta F4}$ mice (Fig. 2a, rows 1 and 2). However, NK cells (NK1.1^{+}) and pDCs (Ly6C^{+}) were found to be selectively absent in *Ikzf1*$^{\Delta F4/\Delta F4}$ mice (similar to their absence in *Ikzf1*^{null} mice), with only slightly reduced numbers of pre-pro-B cells (Fig. 2a, row 3; Fig. 2b, top). Both mutant strains also contained relatively normal percentages and numbers of pro-B and pre-BI cells (Fig. 2a, row 2; Fig. 2b, bottom).

In contrast to the similar numbers of early progenitor cells in the two strains, large pre-BII cells were substantially decreased in *Ikzf1*$^{\Delta F1/\Delta F1}$ mice, yet were increased in *Ikzf1*$^{\Delta F4/\Delta F4}$ mice (Fig. 2a, row 2; Fig. 2b, bottom). Staining for cytoplasmic Ig μ, which is expressed in the majority of large pre-BII cells, confirmed the developmental block in *Ikzf1*$^{\Delta F1/\Delta F1}$ mice, as only a small number of B220^{+}IgM^{-}Igμ^{+} cells were present (Fig. 2c,d). Importantly, an essential role for Ikaros at this developmental stage was previously suggested[7].

Consistent with the deficiency in large pre-BII cells in *Ikzf1*$^{\Delta F1/\Delta F1}$ mice, greatly reduced numbers of small pre-BII, immature and mature recirculating B cells were observed (Fig. 2a, rows 1 and 4; Fig. 2b, bottom). In *Ikzf1*$^{\Delta F4/\Delta F4}$ mice, the numbers of cells in these populations were reduced to a lesser degree. Notably, although much of B cell development appears to be largely intact in *Ikzf1*$^{\Delta F4/\Delta F4}$ mice, its Lin$^{neg–lo}$c-Kit^{+} early progenitors expressed less Flt3 and IL-7Rα (Fig. 2e,f). This phenotype is reminiscent of *Ikzf1*^{null} mice,

although, in the *Ikzf1*$^{\Delta F4/\Delta F4}$ mice, expression of these proteins apparently is not reduced to a sufficient extent to block development.

Additional finger-specific functions in hematopoiesis

Developmental abnormalities observed during T cell development were far more severe in *Ikzf1*$^{\Delta F4/\Delta F4}$ mice than *Ikzf1*$^{\Delta F1/\Delta F1}$ mice. Both strains exhibited slightly reduced thymic cellularity, with a greater reduction in *Ikzf1*$^{\Delta F4/\Delta F4}$ mice (Fig. 3a). During the double-negative (DN) stages of thymopoiesis, reduced cell numbers were readily apparent in *Ikzf1*$^{\Delta F4/\Delta F4}$ mice, but not in *Ikzf1*$^{\Delta F1/\Delta F1}$ mice. The DN1 population (CD44$^+$CD25$^-$)[43] appeared to be reduced in the *Ikzf1*$^{\Delta F1/\Delta F1}$ strain (Fig. 3b and Supplementary Fig. 3a). However, this reduction was due to greatly reduced numbers of other cell types that contaminate the DN1 population, including thymic B cells (see below). Consistent with this interpretation, normal percentages of early thymic progenitor (ETP) cells were found in *Ikzf1*$^{\Delta F1/\Delta F1}$ mice, but were reduced in *Ikzf1*$^{\Delta F4/\Delta F4}$ mice (Fig. 3c). DN2 (CD44$^+$CD25$^+$) and DN3 (CD44$^-$CD25$^+$) cells were also greatly reduced in *Ikzf1*$^{\Delta F4/\Delta F4}$ mice, but were normal in *Ikzf1*$^{\Delta F1/\Delta F1}$ mice (Fig. 3b and Supplementary Fig. 3b,c). Proliferative DN4 cells (CD44$^-$CD25$^-$) recovered in the *Ikzf1*$^{\Delta F4/\Delta F4}$ strain to percentages and numbers comparable to those observed in wild-type mice (Fig. 3b and Supplementary Fig. 3d). The ratio of double-positive (DP) thymocytes to CD4$^+$ or CD8$^+$ single-positive (SP) thymocytes was comparable to wild-type in *Ikzf1*$^{\Delta F1/\Delta F1}$ mice but was significantly reduced in *Ikzf1*$^{\Delta F4/\Delta F4}$ mice (Fig. 3d and Supplementary Fig. 3e). The reduced numbers of DP thymocytes in *Ikzf1*$^{\Delta F4/\Delta F4}$ mice correlated with a clear reduction in the size of the thymic cortex (Fig. 3e). Neither strain exhibited the extreme skewing toward the CD4$^+$ lineage that characterizes *Ikzf1*^{null} mice (Fig. 3d and Supplementary Fig. 3f)[1].

Ikzf1^{null} mice contain reduced numbers of thymic γδ T cells[1]. These cells were largely unperturbed in *Ikzf1*$^{\Delta F1/\Delta F1}$ mice and increased in *Ikzf1*$^{\Delta F4/\Delta F4}$ mice (Fig. 3f). The thymocyte analysis also revealed a severe reduction in thymic B cells (CD19$^+$CD4$^-$CD8$^-$) in *Ikzf1*$^{\Delta F1/\Delta F1}$ mice (Fig. 3g). This selective and consistent phenotype is difficult to explain, given the comparable numbers of conventional B2 B cells in the spleen of the two mutant strains. Furthermore, an examination of the peritoneal cavity revealed reduced numbers of the B1a population in both mutant strains and a reduced number of B1b cells only in the *Ikzf1*$^{\Delta F1/\Delta F1}$ strain (Supplementary Fig. 3g,h). Further analysis of these phenotypes may provide insight into the developmental origin, homing mechanism, and/or function of thymic B cells and peritoneal B1 cells.

Although adult mutant mice contained substantial numbers of mature B and T cells, the *Ikzf1*$^{\Delta F4/\Delta F4}$ strain lacked both B and T lineage cells in the fetus (Fig. 3h-j and Supplementary Fig. 4a-c). In contrast, fetal T cell numbers were normal and fetal B cells were only moderately reduced in the *Ikzf1*$^{\Delta F1/\Delta F1}$ strain. Lymphoid tissue inducer cells (LTi cells, CD45$^+$CD3ε$^-$CD4$^+$IL-7Rα$^+$) were also selectively absent from the fetal intestinal mesentery of *Ikzf1*$^{\Delta F4/\Delta F4}$ mice (Fig. 3k). This phenotype correlated with the selective absence of lymph nodes (inguinal and lumbar) and Peyer's Patches in adult *Ikzf1*$^{\Delta F4/\Delta F4}$ mice, consistent with the important role of fetal LTi cells in the development of these lymphoid structures[1,44] (Fig. 3l and Supplementary Fig. 4d). Nasal-associated lymphoid

tissue (NALT), which develops post-natally[44], was intact (Supplementary Fig. 4e). These phenotypes are reminiscent of those described for *Ikzf1*^{null} mice[1], suggesting that zinc finger 4 is required for the proper regulation of genes involved in early stages of fetal lymphopoiesis. Importantly, finger 1 and all other residues encoded by exon 4 appear to be dispensable for these developmental events.

Finger-specific DNA binding *in vivo*

Generation of the *Ikzf1*$^{\Delta F1/\Delta F1}$ and *Ikzf1*$^{\Delta F4/\Delta F4}$ strains was inspired by evidence that fingers 1 and 4 support the binding to different DNA sequences *in vitro*[29-31]. To determine whether the two fingers also participate in binding to different DNA sequences *in vivo*, we performed ChIP-Seq with total thymocytes from 4-week-old wild-type, *Ikzf1*$^{\Delta F1/\Delta F1}$ and *Ikzf1*$^{\Delta F4/\Delta F4}$ mice.

The most prominent ChIP-Seq peaks were observed at simple repetitive elements that contain multiple sequences with the core Ikaros consensus, GGGAA (Fig. 4a-d). Some of these simple repeats are located in close proximity to protein-coding genes, but the repeats are not conserved through evolution and therefore may not carry out important functions. Nevertheless, the ChIP-Seq profiles confirm that fingers 1 and 4 contribute to differential DNA binding *in vivo*. For example, a repeat region within the *Snx29* gene exhibited a prominent ChIP-Seq peak in wild-type thymocytes and in thymocytes from both mutant strains (Fig. 4a), suggesting that fingers 2 and 3 are sufficient for binding to this region. In contrast, a prominent ChIP-Seq peak within the *Nr3c2* gene was observed in wild-type and *Ikzf1*$^{\Delta F4/\Delta F4}$ thymocytes, but not in *Ikzf1*$^{\Delta F1/\Delta F1}$ thymocytes (Fig. 4b). At a repeat region adjacent to the *Snx25* gene (Fig. 4d), and at a repeat in chromosome 19 that is not linked to an annotated gene (Fig. 4c), strong ChIP-Seq peaks were observed in wild-type and *Ikzf1*$^{\Delta F1/\Delta F1}$ thymocytes, but not in *Ikzf1*$^{\Delta F4/\Delta F4}$ thymocytes.

Inspection of the repeats revealed sequences containing the Ikaros consensus, GGGAA, but with different flanking nucleotides. Motif analyses of the *Snx29* and Nr3c2 regions revealed two repetitive sequences that may support Ikaros binding, while one repetitive sequence likely to support Ikaros binding was found at the *Snx25* and chromosome 19 regions (Fig. 4). *In vitro* binding site selection experiments previously suggested that finger 1 recognizes a pyrimidinerich sequence downstream of the Ikaros core[29] (S.W. and S.T.S., unpublished data). On the basis of those studies, finger 1 would be predicted to bind the TCC sequence within one of the *Nr3c2* repeats (Fig. 4b, bottom right). The other *Nr3c2* consensus (Fig. 4b, bottom left) and the two *Snx29* consensus sequences (Fig. 4a) may also contact finger 1, but perhaps more weakly because the nucleotides that would be contacted by finger 1 include a purine. In contrast, the *Snx25* and chromosome 19 repeats (Fig. 4c,d) are predicted to possess little capacity to interact with finger 1 because the GGGAA core is followed by purines.

The binding site selection data[29] and our recent findings (S.W. and S.T.S., unpublished) failed to reveal a strong DNA sequence preference for finger 4. Instead, finger 4 appears to stabilize binding in a DNA sequence-independent manner, with its DNA contacts particularly important at sites that are not stably bound by fingers 2 and 3 alone (S.W. and S.T.S., unpublished). We hypothesize that finger 4 may be important at the *Snx25* and

chromosome 19 repeats because the DNA-binding energy of fingers 2 and 3 is likely to be weakened by the presence of a purine just downstream of the GGGAA core; our recent studies have shown that a pyrimidine at this position is important for stable protein-DNA interactions by fingers 2 and 3 (S.W. and S.T.S., unpublished).

To determine whether the differential binding observed by ChIP-Seq is due to intrinsic DNA-binding preferences, electrophoretic mobility shift assays (EMSAs) were performed with recombinant proteins containing different combinations of zinc fingers. Consistent with the ChIP-Seq results, substantial binding to one of the *Snx29* sequences was observed with a protein containing all four fingers, as well as with proteins containing only fingers 1-3 or 2-4 (Fig. 4e). The second *Snx29* repeat (with a GaGAA core instead of the GGGAA core) was unable to bind any of the proteins (Supplementary Fig. 5a). Substantial binding to one of the *Nr3c2* sequences was observed with proteins containing fingers 1-4 or 1-3, but not fingers 2-4, demonstrating finger 1-dependent binding (Fig. 4e). Finally, substantial binding to the *Snx25* repetitive sequence was observed with proteins containing fingers 1-4 or fingers 2-4, but not fingers 1-3 (Fig. 4e). Thus, intrinsic *in vitro* binding capacity mirrors the *in vivo* ChIP-Seq results.

In addition to the prominent interactions shown in Figure 4, the ChIP-Seq results revealed thousands of other Ikaros binding sites throughout the genome. More than 60% of the ChIP-Seq peaks coincided with an Ikaros core sequence, GGGAA (Fig. 4f and Supplementary Fig. 5b). In several experiments performed with wild-type or mutant thymocytes, the number of called peaks varied from about 1,000 to 17,000. These numbers are in the same range as the 7,000 Ikaros peaks in thymocytes reported by Zhang *et al*.[16], with extensive overlap observed between the peaks in our experiments and those reported previously. *Zfp64*, *Zfp260*, *Cd4*, *Notch1*, *Hdac7*, and *Bcl11b are* examples of genes exhibiting the same Ikaros peaks in our experiments and in published reports[16,18,19] (Supplementary Fig. 5c). Motif enrichment analysis revealed that the core Ikaros recognition sequence, GGGAA, is highly prevalent at peaks that overlap in the wild-type data set and in the data sets from both mutant strains (Supplementary Fig. 5d). More importantly, the sequence GGGAAAAGGGAA is prevalent at peaks that are selectively absent in the *Ikzf1*$^{\Delta F4/\Delta F4}$ sample (Supplementary Fig. 5d). This sequence is very similar to the sequences in Fig. 4c,d that exhibited finger 4-dependence, suggesting that finger 4 is broadly important for binding to such sequences throughout the genome. Thus, the ChIP-Seq data support a model in which the different functions of fingers 1 and 4 are due, at least in part, to their ability to facilitate binding to distinct genomic sites (see Discussion).

Selective misregulation of gene expression

Although thousands of Ikaros binding sites were identified by ChIP-Seq, the highly selective phenotypes of the *Ikzf1*$^{\Delta F1/\Delta F1}$ and *Ikzf1*$^{\Delta F4/\Delta F4}$ strains suggested that DNA-binding fingers 1 and 4 contribute to the regulation of distinct sets of genes. To examine the roles of fingers 1 and 4 in transcriptional control, we performed RNA-Seq with mRNA from sorted CD4^{+}CD8^{+} thymocytes from 4-week-old wild-type, *Ikzf1*$^{\Delta F1/\Delta F1}$, and *Ikzf1*$^{\Delta F4/\Delta F4}$ mice. The results revealed misregulation of small number of genes in each of the mutant strains. In *Ikzf1*$^{\Delta F4/\Delta F4}$ thymocytes, only 110 genes and 12 genes (with RPKM values ≥4) were

upregulated and downregulated, respectively, by more than 3-fold, with only 24 and 21 genes upregulated and downregulated, respectively, by this magnitude in *Ikzf1*$^{\Delta F1/\Delta F1}$ thymocytes (Fig. 5a and Supplementary Fig. 6). Importantly, only 15 genes were upregulated in both mutant strains and one gene was downregulated in both strains. Three genes that were upregulated in *Ikzf1*$^{\Delta F4/\Delta F4}$ thymocytes were downregulated in *Ikzf1*$^{\Delta F1/\Delta F1}$ thymocytes. Notably, much smaller numbers of genes were upregulated or downregulated by 10-fold or more (Fig. 5b and Supplementary Fig. 6).

Although it is difficult to accurately compare RNA-Seq data sets to microarray data sets, many of the genes found by RNA-Seq to be misregulated in *Ikzf1*$^{\Delta F1/\Delta F1}$ or *Ikzf1*$^{\Delta F4/\Delta F4}$ thymocytes were recently found by microarray to be misregulated in *Ikzf1*^{null} thymocytes[16]. Thus, misregulated genes in *Ikzf1*^{null} thymocytes appear to represent a composite of the genes misregulated in the *Ikzf1*$^{\Delta F1/\Delta F1}$ and *Ikzf1*$^{\Delta F4/\Delta F4}$ thymocytes.

Gene ontology analysis of genes upregulated 3-fold or more in *Ikzf1*$^{\Delta F4/\Delta F4}$ thymocytes revealed enrichment for genes involved in cell adhesion, cell communication and signal transduction (Fig. 5c). Consistent with the invasive properties of the thymic lymphomas that arise in older *Ikzf1*$^{\Delta F4/\Delta F4}$ mice (see below), several genes implicated in tumor invasion and metastasis were among the most potently upregulated genes, including the matrix metalloprotease gene, *Mmp14*, the catenin gene, *Ctnnd1*, and the guanine nucleotide exchange factor gene, *Dock1* (Supplementary Fig. 6e,g)[45-48].

Interestingly, genes that were upregulated in either *Ikzf1*$^{\Delta F1/\Delta F1}$ or *Ikzf1*$^{\Delta F4/\Delta F4}$ thymocytes were generally expressed at very low levels in wild-type thymocytes (Fig. 5d). We depict the distribution by expression level (RPKM) in thymocytes of all annotated genes (Fig. 5d, left), and RPKM distribution in wild-type cells of genes that were upregulated by at least 3-fold in *Ikzf1*$^{\Delta F1/\Delta F1}$ or *Ikzf1*$^{\Delta F4/\Delta F4}$ thymocytes (P<0.001) (Fig. 5d, middle and right). Since the vast majority of upregulated genes were upregulated from a very low expression level, the results are consistent with evidence that Ikaros often functions as a transcriptional repressor.

Zinc finger requirements for tumor suppression

Previously described *Ikzf1* mutant strains develop thymic lymphoma[10,11]. Importantly, we have never observed lymphoma in *Ikzf1*$^{\Delta F1/\Delta F1}$ mice, but *Ikzf1*$^{\Delta F4/\Delta F4}$ mice developed thymic lymphoma with a penetrance similar to that observed in other Ikaros mutant strains (Fig. 6a). Also similar to other *Ikzf1* mutant strains, the lymphomas in *Ikzf1*$^{\Delta F4/\Delta F4}$ mice were aggressive (highly invasive and metastatic) (Fig. 6b,c) and they displayed variable CD4 and CD8 expression (Fig. 6d), clonal TCRβ rearrangement, and aberrant expression of the Notch intracellular domain (ICD) (data not shown).

Ikzf1 mutations in a mouse model of BCR-ABL^{+} B-ALL

Although *Ikzf1* mutations invariably give rise to T cell malignancies in mice, human malignancies of T cell origin rarely contain *IKZF1* mutations[49]. Instead, human *IKZF1* mutations are frequently associated with BCR-ABL^{+} B-ALL and other progenitor-B cell malignances[12,13]. To examine this species difference, and with the additional goal of

developing models to study progenitor-B cell malignancies associated with *IKZF1* mutations, we first made use of a well-established *in vitro* culture assay for BCR-ABL$^+$ B-ALL[50]. Bone marrow cells from wild-type, *Ikzf1*$^{\Delta F1/\Delta F1}$ and *Ikzf1*$^{\Delta F4/\Delta F4}$ mice were transduced with a BCR-ABL-expressing retrovirus and cell numbers in the progenitor B cell cultures were monitored over the course of approximately three weeks. *Ikzf1*$^{\Delta F4/\Delta F4}$ cells transduced with the BCR-ABL retrovirus proliferated much more rapidly than transduced wild-type cells (Fig. 7a). Interestingly, transduced *Ikzf1*$^{\Delta F1/\Delta F1}$ cells proliferated more slowly than the wild-type cells and eventually stopped growing (Fig. 7a and data not shown).

We next employed an *in vivo* model of BCR-ABL$^+$ B-ALL in which BCR-ABL-transduced bone marrow cells were transplanted into irradiated wild-type C57BL/6 recipients. In this assay, BCR-ABL-transduced cells from *Ikzf1*$^{\Delta F4/\Delta F4}$ mice yielded much more aggressive malignancies than transduced cells from wild-type or *Ikzf1*$^{\Delta F1/\Delta F1}$ mice (Fig. 7b). These results demonstrate that an *Ikzf1* mutation can contribute to B cell malignancy in mice when combined with BCR-ABL expression. Furthermore, the results establish an important parallel between the tumor suppressor function of Ikaros in thymocytes and progenitor-B cells; in both cell types, finger 4 is essential for tumor suppression, whereas finger 1 is dispensable.

To approach an understanding of the tumor suppressor function of Ikaros, RNA-Seq was performed with mRNA from BCR-ABL-transduced cells cultured for 21 or 28 days. We also performed RNA-Seq with sorted pro-B and pre-BI+large pre-BII cells, which are thought to most closely represent the developmental stages that expand following BCR-ABL transformation. Cluster analysis revealed extensive differences in gene expression between the normal and transformed cells (Fig. 7c). However, most of the gene expression changes were unaffected by the *Ikzf1* mutations. Clusters 1-3, for example, show differences between all of the data sets from untransformed cells in comparison to all of the data sets from transformed cells. Gene ontology analysis of the two largest clusters, Clusters 1 and 2, revealed, as expected, that cell cycle and cell growth control genes were often upregulated upon BCR-ABL transformation, whereas genes involved in leukocyte differentiation and activation were downregulated (Supplementary Fig. 7).

The remaining three clusters (Fig. 7c, Clusters 4-6) contain genes that were more abundantly expressed in BCR-ABL-transformed cells from *Ikzf1*$^{\Delta F1/\Delta F1}$ mice, in comparison to wild-type and *Ikzf1*$^{\Delta F4/\Delta F4}$ mice. These same genes were expressed more abundantly in untransformed pre-BI+large pre-BII cells from *Ikzf1*$^{\Delta F1/\Delta F1}$ mice, suggesting that the *Ikzf1*$^{\Delta F1/\Delta F1}$ cells that proliferate in culture following BCR-ABL transformation are maintained at the pre-BI to large pre-BII developmental stage, a stage at which many genes are misregulated in *Ikzf1*$^{\Delta F1/\Delta F1}$ mice. Importantly, most genes in all six clusters in Figure 7c were similarly expressed in the wild-type and *Ikzf1*$^{\Delta F4/\Delta F4}$ samples, despite the greatly enhanced proliferation of BCR-ABL transformed *Ikzf1*$^{\Delta F4/\Delta F4}$ cells.

To identify genes that were selectively misregulated in BCR-ABL-transformed *Ikzf1*$^{\Delta F4/\Delta F4}$ cells, an additional cluster analysis was performed with the six data sets obtained with transformed cells; the expression levels from untransformed cells were then aligned after the

clusters were defined (Fig. 7d). This analysis revealed 155 genes that were selectively upregulated, and 133 genes that were selectively downregulated, in both the day-21 and day-28 *Ikzf1*$^{\Delta F4/\Delta F4}$ cultures in comparison to the wild-type and *Ikzf1*$^{\Delta F1/\Delta F1}$ cultures. Among the genes that were expressed more abundantly in the *Ikzf1*$^{\Delta F4/\Delta F4}$ cells was *Kit* (Fig. 7d,f), which is known to be silenced during B cell maturation. Among the genes that were expressed less abundantly were *Il2ra* (CD25) and *Enpep* (BP-1), which are activated during B cell maturation (Fig. 7d,f). Flow cytometry confirmed the misregulation of the c-Kit and CD25 (IL-2Rα) proteins (Fig. 7e). These findings suggest that the *Ikzf1*$^{\Delta F4/\Delta F4}$ mutation may influence the developmental stage of cells transformed by BCR-ABL. However, most of the other genes that were selectively misregulated in the BCR-ABL transformed *Ikzf1*$^{\Delta F4/\Delta F4}$ cells are not developmentally regulated, and several, such as *Dock1* and *Ctnnd1*, correspond to genes that were misregulated also in *Ikzf1*$^{\Delta F4/\Delta F4}$ thymocytes. The identification of a limited set of genes that are selectively misregulated in transformed cells in the context of the *Ikzf1*$^{\Delta F4/\Delta F4}$ mutation provides an important step toward dissection of the elusive mechanisms responsible for the tumor suppressor function of Ikaros.

Discussion

We have created two new mouse strains in which exons encoding individual zinc fingers of Ikaros were deleted. The results demonstrate that different zinc fingers within a single DNA-binding domain can participate in the regulation of distinct sets of genes and contribute to distinct biological functions. The disruption of individual fingers may be a generally valuable strategy for dissecting the complex biological functions and mechanisms of action of zinc finger transcription factors.

When designing the mutant strains, we considered three different strategies: deletion of the exons encoding fingers 1 and 4, deletion of fingers 1 and 4 while retaining the other residues encoded by their respective exons, or mutagenesis of key residues involved in DNA-binding. Each strategy had notable advantages and limitations. An advantage of the second and third strategies is that it would be possible to exclude the involvement of non-finger residues in the resulting phenotypes. However, a major limitation of these strategies is that the mutant proteins do not normally exist in murine cells, raising the possibility of dominant negative or gain-of-function activities. Consistent with this possibility, a point mutation in Ikaros zinc finger 3 was previously found to have much stronger dominant negative properties in mice than a deletion mutant that completely removed the exons encoding fingers 1, 2 and 3 (ref. 51). Furthermore, preliminary data suggest that exon 4-encoded residues immediately upstream of finger 1 autoregulate finger 1's DNA-binding activity (S.W. and S.T.S., unpublished results); retention of these residues while deleting finger 1 would have an uncertain outcome.

Because of the above limitations, we deleted exons 4 and 6, including fingers 1 and 4, respectively, and the small number of additional residues encoded by these exons. With this strategy, it remains possible that some of the phenotypes are due to the loss of activities other than the DNA-binding activity of the deleted finger. However, we can conclude with confidence that finger 1 and finger 4 are fully and differentially dispensable for several biological functions of Ikaros, and the data strongly suggest that at least a subset of the

phenotypes of each strain are due to loss of finger-dependent DNA interactions. Furthermore, the *Ikzf1*$^{\Delta F1/\Delta F1}$ strain reveals the specific functions of full-length Ik-1, as this strain lacks the Ik-1 isoform while retaining the naturally occurring Ik-2 isoform. Most importantly, since the long-term goal is to dissect the highly selective phenotypes of the mutant strains for the purpose of understanding how Ikaros regulates lymphopoiesis and leukemogenesis, we can proceed with relatively little concern about the possibility of aberrant gain-of-function activities.

We were surprised to find that the two fingers regulate different biological functions and even different steps within the same developmental pathway. We originally anticipated that Ikaros would regulate numerous genes involved in each developmental step in which it participates, such that each mutant strain would exhibit similar phenotypes as *Ikzf1*^{null} mice. This expectation was based on evidence that gene expression is substantially altered in *Ikzf1*^{null} cells[16,20] and that Ikaros binds several thousand genomic sites in ChIP-Seq experiments[16]. Instead, we found that finger 1 is largely or fully dispensable for many biological functions of Ikaros, with finger 4 dispensable for several other functions.

This striking selectivity provides strong support for a hypothesis in which only one or a small number of target genes is essential for each biological event in which Ikaros participates. It is difficult to envision that Ikaros would be a critical regulator of hundreds of genes required for each biological event, with finger 1 dispensable for the regulation of all target genes involved in some events and finger 4 dispensable for the regulation of all genes involved in other events. Instead, it seems much more likely that each event requires the proper regulation of only one or a few Ikaros target genes, with either finger 1 or finger 4 critical for the regulation of those genes. Although we favor a model in which Ikaros is an essential regulator of only a few key genes involved in each biological event, an alternative possibility is that fingers 2 and 3 are sufficient for the regulation of almost all critical target genes involved in each of its biological functions, with fingers 1 or 4 essential for the regulation of only a few key genes.

A long-standing challenge in the transcription field has been to identify direct targets of transcription factors that can explain their biological functions. Efforts to identify transcription factor targets have benefited greatly from the development of gene expression profiling methods and methods for examining DNA-binding *in vivo* at a genome-wide scale (e.g. ChIP-Seq). By merging ChIP-Seq data with gene expression profiles from wild-type and knockout cells, insights into the direct targets of a transcription factor can be obtained. However, a major limitation of this approach is that many transcription factors may bind genomic sites at which they do not function[52]. Moreover, because some transcription factors may preferentially bind sequences associated with the relatively open chromatin found at active promoters and enhancers, it can be difficult to conclude with confidence that the merger of gene expression and ChIP data sets have successfully identified the direct functional targets.

In our RNA-Seq studies, we found that most misregulated genes in *Ikzf1*$^{\Delta F1/\Delta F1}$ and *Ikzf1*$^{\Delta F4/\Delta F4}$ thymocytes were expressed at low levels in wild-type cells, whereas Ikaros binding sites defined by ChIP-Seq were distributed among genes at all expression levels

(data not shown). Furthermore, the number of ChIP-Seq peaks greatly exceeded the number of misregulated genes. One possible and perhaps likely interpretation of these results is that most Ikaros binding sites identified by ChIP-Seq are not functionally relevant. However, many other possibilities must be considered. For example, Ikaros may contribute to the proper regulation of a much larger number of genes, but its absence may alter the expression level of most target genes by a magnitude that fails to reach the 3-fold cutoff used for our analyses. Another possibility is that Ikaros acts redundantly with other Ikaros family members at many of its target genes.

We originally were hopeful that ChIP-Seq experiments with our mutant strains would reveal a clear loss of Ikaros binding to a well-defined subset of sites, leading to an improved correlation between binding and transcriptional misregulation of nearby genes. However, although we observed reduced numbers of ChIP-Seq peaks with *Ikzf1*$^{\Delta F1/\Delta F1}$ and *Ikzf1*$^{\Delta F4/\Delta F4}$ thymocytes (data not shown), we have been unable to perform a meaningful analysis of the binding events that require or are enhanced by these fingers. A primary reason for this difficulty is that the ChIP-Seq peaks are not clearly polarized, in that we do not observe a clear subset of peaks that are entirely dependent on finger 4 and another subset of peaks that are entirely dependent on finger 1. Instead, a continuum of effects was observed, with differential yet highly variable degrees of dependence on finger 1 or finger 4.

The potential value of targeting individual zinc fingers can be summarized as follows. First, the *Ikzf1*$^{\Delta F1/\Delta F1}$ and *Ikzf1*$^{\Delta F4/\Delta F4}$ mutant mice exhibited select subsets of the phenotypes observed in *Ikzf1*^{null} mice. Second, when a phenotype was observed, it was found to be as robust or nearly as robust as that observed in the *Ikzf1*^{null} mice, thereby making the phenotype amenable to further analysis. Third, despite the robust phenotypes, gene expression changes were quite limited, thereby narrowing the list of potential direct and indirect target genes responsible for the phenotype. These findings pave the way for detailed analyses of each phenotype observed in the mutant strains.

Our results raise the question of why Ikaros and perhaps other zinc finger transcription factors acquired the capacity to bind DNA through different subsets of their fingers. One possibility is that this strategy allows Ikaros to recognize a larger number of DNA sequences, such that each target gene does not need to possess a sequence that matches a single, rigid consensus. Although this simple scenario is possible, we favor a model in which recognition of DNA through different combinations of fingers supports different functions. One possibility is that binding to DNA through different combinations of zinc fingers leads to conformational differences in the bound protein that may influence co-regulatory interactions. The zinc finger DNA-binding protein, CTCF, has similarly been suggested to carry out different functions when bound to DNA through different subsets of its fingers[40], yet this hypothesis has not yet been tested through the disruption of individual CTCF fingers.

Finally, it can be argued that the most important function of Ikaros to understand is its tumor suppressor function. The correlation between *IKZF1* mutations and the therapeutic response of high-risk progenitor-B-ALL suggests that an understanding of the tumor suppressor function may be critical for the development of new therapies[12,13]. The establishment of a

mouse model for BCR-ABL$^+$ B-ALL using the *Ikzf1*$^{\Delta F4/\Delta F4}$ strain confirms a recent report that B cell malignancies can be observed in an *Ikzf1* mutant strain when coupled to BCR-ABL expression[53]. The finding that finger 4 is selectively required for tumor suppression both in thymocytes and in the BCR-ABL$^+$ B-ALL model suggests that tumor suppression in the two cell types may involve similar molecular mechanisms. This hypothesis is further supported by the finding that many of the same genes are misregulated in *Ikzf1*$^{\Delta F4/\Delta F4}$ thymocytes and in BCR-ABL-transformed progenitor B cells from *Ikzf1*$^{\Delta F4/\Delta F4}$ mice. The loss of the tumor suppressor function of Ikaros in the *Ikzf1*$^{\Delta F4/\Delta F4}$ strain will make this strain particularly valuable for future studies, since it exhibits only a subset of the other phenotypes observed in *Ikzf1*^{null} mice. This feature will allow studies of the tumor suppressor function in a background in which many Ikaros target genes involved in its other functions are relatively unperturbed.

Online Methods

Methods and any associated references are available in the online version of the paper at http://www.nature.com/natureimmunology/.

Methods

Mice

Germline-targeted deletions of exon 4 (encoding zinc finger 1) and exon 6 (encoding zinc finger 4) of the *Ikzf1* gene were obtained by homologous recombination in embryonic stem cells (ESC). Electroporation of ESC was performed in the UCLA Molecular Genetic Technology Center (MGTC) and screening for correctly targeted ESC clones was performed by Southern blot. Injection of the mutant ESC lines into 129 blastocysts was performed by the UCLA MGTC. After germline transmission was achieved, the floxed *neo*^{r} cassette introduced into the genome during homologous recombination was removed by crossing with *EIIa*-cre mice on a C57BL/6 background. Germline transmission of the deletions was confirmed after backcrossing with wild-type C57BL/6 mice. The mutant strains were subsequently backcrossed through more than 10 generations with wild-type C57BL/6. Animals were excluded from analysis of hematopoietic development if they were runt, or if they had developed thymic lymphoma (for the *Ikzf1*$^{\Delta F4/\Delta F4}$ strain). No randomization or blinding was performed for the animal studies. Animals of both sexes were used, at E18.5 (fetal hematopoiesis), 4 weeks (thymic development) and 6-8 weeks of age (peripheral lymph nodes, peritoneal B cells, spleen and bone marrow). All phenotypes described were analyzed with a minimum sample size $n = 5$, using wild-type littermate controls and represented by at least 3 separate experiments with animals from different litters. Animals were housed in the vivaria of the UCLA Division of Laboratory Animal Medicine. All experiments were approved by the UCLA Animal Research Committee (ARC) and were performed according to UCLA Institutional Animal Care and Use Committee guidelines. Wild-type C57BL/6 and *EIIa*-cre mice were purchased from The Jackson Laboratory.

Cell preparations and flow cytometry

Cell suspensions were prepared from adult hematopoietic tissues and filtered through 70 μm nylon cell strainers (BD Biosciences). Fetal hematopoietic cells were prepared as previously described from mesentery[54] and fetal liver[55]. All antibodies for flow cytometry were from BD Biosciences or eBioscience, except for the cytoplasmic Ig μ antibody, which was from Southern Biotech (Supplementary Table 1). All antibodies were initially used at 1:200 dilutions and were individually titrated when necessary. Intracellular staining of cytoplasmic μ was performed using reagents from the Foxp3 staining buffer set (eBioscience). Flow cytometry or sorting was performed on a FACSCalibur, BD LSR II, or FACSAria II SOP (BD Biosciences), and data were analyzed using FlowJo 7.5 and Diva 6.1.1 software.

Histological analysis and visualization of lymph nodes and Peyer's patches

Dissected tissues were fixed in 10% formalin (4% formaldehyde) (Fisher Scientific) for > 72 h, decalcified when needed, embedded in paraffin, sectioned, and stained with hematoxylin and eosin (H&E) by the Translational Pathology Core Laboratory at UCLA. Visualization of inguinal and lumbar lymph nodes and Peyer's patches was done as described[54,56].

Immunoblots

Whole cell extracts were prepared by re-suspension of cells in 1 volume water in the presence of protease inhibitor cocktail (Roche) and immediate direct lysis by adding 1 volume of 2× SDS sample buffer. SDS-polyacrylamide gel electrophoresis and transfer to nitrocellulose membrane were performed, and blots were probed with an antibody raised against the N-terminal region of Ikaros (residues 1-80)[32] or an antibody against SNP70[57] as loading control.

Retroviral transduction, cell culture, and bone marrow transplantation

Retroviral supernatants for expression of BCR-ABL were produced with the pMSCV-YFP-IRES-p185 plasmid, and bone marrow cells were transduced as described[50], except that whole bone marrow from untreated mice was used for transduction. For *in vitro* cell culture, 5×10^6 transduced cells were plated on top of pre-established feeder cells from wild-type C57BL/6 bone-marrow stroma. Cells were split, counted, and reseeded at 1-2 $\times 10^5$ cells/ml in 5 ml every 2-3 days for growth curve analysis. For *in vivo* experiments, 1×10^6 transduced whole bone marrow cells were injected intravenously into irradiated wild-type C57BL/6 recipient mice. Mice were monitored for development of B-ALL, and the end-point was assessed by complete paralysis of hind legs or moribund condition.

RNA purification and RNA-Seq

RNA was prepared using TRI Reagent (Molecular Research Center, Inc.) followed by purification with an RNeasy kit (Qiagen), with on-column RNase-free DNase I treatment. For RNA-Seq analysis, MicroPoly(A)Purist Kit (Ambion) or the Tru-Seq RNA Sample Prep Kit (Illumina) was used to isolate mRNA according to the manufacturer's protocol. cDNA was prepared for the Illumina Sequencing platform using the fragmented double-stranded cDNA protocol[58] or using the Illumina TruSeq kit. Sequencing was performed on an Illumina HiSeq machine with 50-bp single-end reads at the UCLA Broad Stem Cell

Research Center High Throughput Sequencing Core. Raw data were uploaded to the Galaxy website (http://galaxy.psu.edu/) and mapped with Tophat to the July 2007 annotation of the mouse (Mus musculus) genome (mm9), filtering for uniquely mapped reads[59-63]. Genome coverage visualization files were created with BEDtools and uploaded to UC Santa Cruz genome browser (http://genome.ucsc.edu)[64]. Relative mRNA expression levels (RPKM)[65] were calculated based on exonic reads using SeqMonk software (Babraham Bioinformatics) and reference genome annotations from NCBI (mm9). For RNA-Seq analysis of DP thymocytes, exonic reads were analyzed by the Bioconductor DESeq program[66] to find genes differentially expressed to a statistically significant degree between two populations. Clustering analysis (k-means) was performed on log2-transformed, mean centered RPKM values, using Cluster 3.0 software[67,68] and visualized with Java Treeview software[69]. Gene ontology analysis was performed using Panther software[70].

ChIP and ChIP-Seq

Primary thymocytes were fixed in 1% formaldehyde for 10 min at 25 °C, washed in PBS and snap frozen. Ikaros ChIP was performed with an antibody directed against the Ikaros N-terminal region (residues 1-80)[32] and tested by PCR for enrichment at published[18,19] and unpublished (Zfp260) Ikaros binding sites identified from initial ChIP-Seq experiments. Input DNA was prepared from wild-type thymocytes as a negative control. Libraries were prepared for sequencing on the Illumina platform as described[71] and sequenced at the USC Epigenome Data Production Facility and the UCLA Broad Stem Cell Research Center High Throughput Sequencing Core. Raw sequences were mapped by Bowtie to the July 2007 annotation of mouse (Mus musculus) genome data (mm9), and significant peaks over background were called using the Sole-Search software[72,73]. Genome coverage visualization files were created with BEDtools and uploaded to the UC Santa Cruz genome browser (http://genome.ucsc.edu)[64]. *De novo* motif analysis was performed using the Homer software[74], and position weight matrix analysis was performed with the MEME software (http://meme.sdsc.edu/meme/intro.html)[75].

Recombinant protein preparation and gel electrophoretic mobility shift assays (EMSA)

Ikzf1 gene sequences encoding DNA-binding zinc fingers 1 through 4 were PCR amplified from cDNA and subcloned into the bacterial expression plasmid pGEX-4T-1 (GE Healthcare) by standard methods. Recombinant proteins were expressed in Rosetta (DE3) (Novagen), induced with IPTG, and purified using B-PER GST Fusion Protein Purification Kit (Thermo Scientific). The GST tags were removed and proteins were purified by on-column thrombin cleavage. Ikaros EMSAs were performed as described[30], with the exception that bacterially expressed recombinant Ikaros proteins were used instead of nuclear extracts. Sequences of probes are given in Supplementary Table 2.

Statistical analysis

Statistical analyses (unpaired, two-tailed, Student's *t* test, 95% confidence intervals) were performed with the GraphPad Prism software.

Supplementary Material

Refer to Web version on PubMed Central for supplementary material.

Acknowledgments

We thank P. Aliahmad (Cedars-Sinai, CA, USA), D. Bhatt, K. Dorshkind, C. Li, and E. Montecino-Rodriguez for helpful advice and/or critical reading of the manuscript, the UCLA Division of Laboratory Animal Medicine (DLAM) for ongoing care of mice, and H. Mak, T. Jacob, C. Garcia, J. Flores and J. Lorenzano for assistance with the mouse colony. ChIP-Seq and RNA-Seq libraries were sequenced at the USC Epigenome Data Production Facility and the UCLA Broad Stem Cell Research Center High Throughput Sequencing Core. This work was supported by NIH grant RO1DK043726 (to S.T.S.). O.N.W. is an Investigator of the Howard Hughes Medical Institute.

References

1. Wang JH, et al. Selective defects in the development of the fetal and adult lymphoid system in mice with an Ikaros null mutation. Immunity. 1996; 5:537–549. [PubMed: 8986714]
2. Georgopoulos K. Haematopoietic cell-fate decisions, chromatin regulation and ikaros. Nat Rev Immunol. 2002; 2:162–174. [PubMed: 11913067]
3. Yoshida T, Ng SY, Georgopoulos K. Awakening lineage potential by Ikaros-mediated transcriptional priming. Curr Opin Immunol. 2010; 22:154–160. [PubMed: 20299195]
4. Yoshida T, Ng SY, Zuniga-Pflucker JC, Georgopoulos K. Early hematopoietic lineage restrictions directed by Ikaros. Nat Immunol. 2006; 7:382–391. [PubMed: 16518393]
5. Kirstetter P, Thomas M, Dierich A, Kastner P, Chan S. Ikaros is critical for B cell differentiation and function. Eur J Immunol. 2002; 32:720–730. [PubMed: 11870616]
6. Thompson EC, et al. Ikaros DNA-binding proteins as integral components of B cell developmental-stage-specific regulatory circuits. Immunity. 2007; 26:335–344. [PubMed: 17363301]
7. Reynaud D, et al. Regulation of B cell fate commitment and immunoglobulin heavy-chain gene rearrangements by Ikaros. Nat Immunol. 2008; 9:927–936. [PubMed: 18568028]
8. Trageser D, et al. Pre-B cell receptor-mediated cell cycle arrest in Philadelphia chromosome-positive acute lymphoblastic leukemia requires IKAROS function. J Exp Med. 2009; 206:1739–1753. [PubMed: 19620627]
9. Ma S, et al. Ikaros and Aiolos inhibit pre-B-cell proliferation by directly suppressing c-Myc expression. Mol Cell Biol. 2010; 30:4149–4158. [PubMed: 20566697]
10. Winandy S, Wu P, Georgopoulos K. A dominant mutation in the Ikaros gene leads to rapid development of leukemia and lymphoma. Cell. 1995; 83:289–299. [PubMed: 7585946]
11. Dumortier A, et al. Notch activation is an early and critical event during T-cell leukemogenesis in Ikaros-deficient mice. Mol Cell Biol. 2006; 26:209–220. [PubMed: 16354692]
12. Mullighan CG, et al. BCR-ABL1 lymphoblastic leukaemia is characterized by the deletion of Ikaros. Nature. 2008; 453:110–114. [PubMed: 18408710]
13. Mullighan CG, et al. Deletion of IKZF1 and prognosis in acute lymphoblastic leukemia. N Eng J Med. 2009; 360:470–480.
14. Kim J, et al. Ikaros DNA-binding proteins direct formation of chromatin remodeling complexes in lymphocytes. Immunity. 1999; 10:345–355. [PubMed: 10204490]
15. Sridharan R, Smale ST. Predominant interaction of both Ikaros and Helios with the NuRD complex in immature thymocytes. J Biol Chem. 2007; 282:30227–30238. [PubMed: 17681952]
16. Zhang J, et al. Harnessing of the nucleosome-remodeling-deacetylase complex controls lymphocyte development and prevents leukemogenesis. Nat Immunol. 2011; 13:86–94. [PubMed: 22080921]
17. Harker N, et al. The CD8alpha gene locus is regulated by the Ikaros family of proteins. Mol Cell. 2002; 10:1403–1415. [PubMed: 12504015]

18. Naito T, Gomez-Del Arco P, Williams CJ, Georgopoulos K. Antagonistic interactions between Ikaros and the chromatin remodeler Mi-2beta determine silencer activity and Cd4 gene expression. Immunity. 2007; 27:723–734. [PubMed: 17980631]
19. Gomez-del Arco P, et al. Alternative promoter usage at the Notch1 locus supports ligand-independent signaling in T cell development and leukemogenesis. Immunity. 2010; 33:685–698. [PubMed: 21093322]
20. Ng SY, Yoshida T, Zhang J, Georgopoulos K. Genome-wide lineage-specific transcriptional networks underscore Ikaros-dependent lymphoid priming in hematopoietic stem cells. Immunity. 2009; 30:493–507. [PubMed: 19345118]
21. John LB, Ward AC. The Ikaros gene family: transcriptional regulators of hematopoiesis and immunity. Mol Immunol. 2011; 48:1272–1278. [PubMed: 21477865]
22. Sun L, Liu A, Georgopoulos K. Zinc finger-mediated protein interactions modulate Ikaros activity, a molecular control of lymphocyte development. EMBO J. 1996; 15:5358–5369. [PubMed: 8895580]
23. Trinh LA, et al. Down-regulation of TDT transcription in CD4(+)CD8(+) thymocytes by Ikaros proteins in direct competition with an Ets activator. Genes Dev. 2001; 15:1817–1832. [PubMed: 11459831]
24. McCarty AS, Kleiger G, Eisenberg D, Smale ST. Selective dimerization of a C2H2 zinc finger subfamily. Mol Cell. 2003; 11:459–470. [PubMed: 12620233]
25. Tupler R, Perini G, Green MR. Expressing the human genome. Nature. 2001; 409:832–833. [PubMed: 11237001]
26. Ravasi T, et al. Systematic characterization of the zinc-finger-containing proteins in the mouse transcriptome. Genome Res. 2003; 13:1430–1442. [PubMed: 12819142]
27. Klug A. The discovery of zinc fingers and their applications in gene regulation and genome manipulation. Annu Rev Biochem. 2010; 79:213–231. [PubMed: 20192761]
28. Wolfe SA, Nekludova L, Pabo CO. DNA recognition by Cys2His2 zinc finger proteins. Annu Rev Biophys Biomol Struct. 2000; 29:183–212. [PubMed: 10940247]
29. Molnar A, Georgopoulos K. The Ikaros gene encodes a family of functionally diverse zinc finger DNA-binding proteins. Mol Cell Biol. 1994; 14:8292–8303. [PubMed: 7969165]
30. Cobb BS, et al. Targeting of Ikaros to pericentromeric heterochromatin by direct DNA binding. Genes Dev. 2000; 14:2146–2160. [PubMed: 10970879]
31. Koipally J, Heller EJ, Seavitt JR, Georgopoulos K. Unconventional potentiation of gene expression by Ikaros. J Biol Chem. 2002; 277:13007–13015. [PubMed: 11799125]
32. Hahm K, et al. Helios, a T cell-restricted Ikaros family member that quantitatively associates with Ikaros at centromeric heterochromatin. Genes Dev. 1998; 12:782–796. [PubMed: 9512513]
33. Payne KJ, et al. Ikaros isoform x is selectively expressed in myeloid differentiation. J Immunol. 2003; 170:3091–3098. [PubMed: 12626565]
34. Miller J, McLachlan AD, Klug A. Repetitive zinc-binding domains in the protein transcription factor IIIA from Xenopus oocytes. EMBO J. 1985; 4:1609–1614. [PubMed: 4040853]
35. Shastry BS. Transcription factor IIIA (TFIIIA) in the second decade. J Cell Sci. 1996; 109:535–539. [PubMed: 8907699]
36. Filippova GN, et al. An exceptionally conserved transcriptional repressor, CTCF, employs different combinations of zinc fingers to bind diverged promoter sequences of avian and mammalian c-myc oncogenes. Mol Cell Biol. 1996; 16:2802–2813. [PubMed: 8649389]
37. Ohlsson R, Renkawitz R, Lobanenkov V. CTCF is a uniquely versatile transcription regulator linked to epigenetics and disease. Trends Genet. 2001; 17:520–527. [PubMed: 11525835]
38. Renda M, et al. Critical DNA binding interactions of the insulator protein CTCF: a small number of zinc fingers mediate strong binding, and a single finger-DNA interaction controls binding at imprinted loci. J Biol Chem. 2007; 282:33336–33345. [PubMed: 17827499]
39. Nurmemmedov E, Yengo RK, Uysal H, Karlsson R, Thunnissen MM. New insights into DNA-binding behavior of Wilms tumor protein (WT1)--a dual study. Biophys Chem. 2009; 145:116–125. [PubMed: 19853363]

40. Nakahashi H, et al. A genome-wide map of CTCF multivalency redefines the CTCF code. Cell Rep. 2013; 3:1678–1689. [PubMed: 23707059]
41. Hardy RR, Carmack CE, Shinton SA, Kemp JD, Hayakawa K. Resolution and characterization of pro-B and pre-pro-B cell stages in normal mouse bone marrow. J Exp Med. 1991; 173:1213–1225. [PubMed: 1827140]
42. Rolink A, Grawunder U, Winkler TH, Karasuyama H, Melchers F. IL-2 receptor alpha chain (CD25, TAC) expression defines a crucial stage in pre-B cell development. Int Immunol. 1994; 6:1257–1264. [PubMed: 7526894]
43. Rothenberg EV, Moore JE, Yui MA. Launching the T-cell-lineage developmental programme. Nat Rev Immunol. 2008; 8:9–21. [PubMed: 18097446]
44. Randall TD, Carragher DM, Rangel-Moreno J. Development of secondary lymphoid organs. Annu Rev Immunol. 2008; 26:627–650. [PubMed: 18370924]
45. Juric D, et al. Differential gene expression patterns and interaction networks in BCR-ABL-positive and -negative adult acute lymphoblastic leukemias. J Clin Oncol. 2007; 25:1341–1349. [PubMed: 17312329]
46. Lu Q. delta-Catenin dysregulation in cancer: interactions with E-cadherin and beyond. J Pathol. 2010; 222:119–123. [PubMed: 20715154]
47. Wang H, et al. The role of Crk/Dock180/Rac1 pathway in the malignant behavior of human ovarian cancer cell SKOV3. Tumour Biol. 2010; 31:59–67. [PubMed: 20237902]
48. Perentes JY, et al. Cancer cell-associated MT1-MMP promotes blood vessel invasion and distant metastasis in triple-negative mammary tumors. Cancer Res. 2011; 71:4527–4538. [PubMed: 21571860]
49. Marcais A, et al. Genetic inactivation of Ikaros is a rare event in human T-ALL. Leuk Res. 2010; 34:426–429. [PubMed: 19796813]
50. Wong S, et al. Sole BCR-ABL inhibition is insufficient to eliminate all myeloproliferative disorder cell populations. Proc Natl Acad Sci USA. 2004; 101:17456–17461. [PubMed: 15505216]
51. Papathanasiou P, et al. Widespread failure of hematolymphoid differentiation caused by a recessive niche-filling allele of the Ikaros transcription factor. Immunity. 2003; 19:131–144. [PubMed: 12871645]
52. Lickwar CR, Mueller F, Hanlon SW, McNally JG, Lieb JD. Genome-wide protein-DNA binding dynamics suggest a molecular clutch for transcription factor function. Nature. 2012; 484:251–255. [PubMed: 22498630]
53. Virely C, et al. Haploinsufficiency of the IKZF1 (IKAROS) tumor suppressor gene cooperates with BCR-ABL in a transgenic model of acute lymphoblastic leukemia. Leukemia. 2010; 24:1200–1204. [PubMed: 20393504]
54. Sun Z, et al. Requirement for RORgamma in thymocyte survival and lymphoid organ development. Science. 2000; 288:2369–2373. [PubMed: 10875923]
55. Montecino-Rodriguez E, Leathers H, Dorshkind K. Identification of a B-1 B cell-specified progenitor. Nat Immunol. 2006; 7:293–301. [PubMed: 16429139]
56. Aliahmad P, de la Torre B, Kaye J. Shared dependence on the DNA-binding factor TOX for the development of lymphoid tissue-inducer cell and NK cell lineages. Nat Immunol. 2010; 11:945–952. [PubMed: 20818394]
57. Pandya-Jones A, Black DL. Co-transcriptional splicing of constitutive and alternative exons. RNA. 2009; 15:1896–1908. [PubMed: 19656867]
58. Nagalakshmi U, Waern K, Snyder M. RNA-Seq: a method for comprehensive transcriptome analysis. Curr Protoc Mol Biol. 2010; 89:4.11.1–4.11.13.
59. Giardine B, et al. Galaxy: a platform for interactive large-scale genome analysis. Genome Res. 2005; 15:1451–1455. [PubMed: 16169926]
60. Trapnell C, Pachter L, Salzberg SL. TopHat: discovering splice junctions with RNA-Seq. Bioinformatics. 2009; 25:1105–1111. [PubMed: 19289445]
61. Blankenberg D, et al. Galaxy: a web-based genome analysis tool for experimentalists. Curr Protoc Mol Biol. 2010; 89:19.10.1–19-10-21.

62. Fujita PA, et al. The UCSC Genome Browser database: update 2011. Nucleic Acids Res. 2010; 39:D876–D882. [PubMed: 20959295]

63. Goecks J, Nekrutenko A, Taylor J. Galaxy: a comprehensive approach for supporting accessible, reproducible, and transparent computational research in the life sciences. Genome Biol. 2010; 11:R86. [PubMed: 20738864]

64. Kent WJ, et al. The human genome browser at UCSC. Genome Res. 2002; 12:996–1006. [PubMed: 12045153]

65. Mortazavi A, Williams BA, McCue K, Schaeffer L, Wold B. Mapping and quantifying mammalian transcriptomes by RNA-Seq. Nat Methods. 2008; 5:621–628. [PubMed: 18516045]

66. Anders S, Huber W. Differential expression analysis for sequence count data. Genome Biol. 2010; 11:R106. [PubMed: 20979621]

67. Eisen MB, Spellman PT, Brown PO, Botstein D. Cluster analysis and display of genome-wide expression patterns. Proc Natl Acad Sci USA. 1998; 95:14863–14868. [PubMed: 9843981]

68. de Hoon MJ, Imoto S, Nolan J, Miyano S. Open source clustering software. Bioinformatics. 2004; 20:1453–1454. [PubMed: 14871861]

69. Saldana AJ. Java Treeview - extensible visualization of microarray data. Bioinformatics. 2004; 20:3246–3248. [PubMed: 15180930]

70. Thomas PD, et al. Applications for protein sequence-function evolution data: mRNA/protein expression analysis and coding SNP scoring tools. Nucleic Acids Res. 2006; 34:W645–W650. [PubMed: 16912992]

71. O'Geen H, Frietze S, Farnham PJ. Using ChIP-seq technology to identify targets of zinc finger transcription factors. Methods Mol Biol. 2010; 649:437–455. [PubMed: 20680851]

72. Langmead B, Trapnell C, Pop M, Salzberg SL. Ultrafast and memory-efficient alignment of short DNA sequences to the human genome. Genome Biol. 2009; 10:R25. [PubMed: 19261174]

73. Blahnik KR, et al. Sole-Search: an integrated analysis program for peak detection and functional annotation using ChIP-seq data. Nucleic Acids Res. 2010; 38:e13. [PubMed: 19906703]

74. Heinz S, et al. Simple combinations of lineage-determining transcription factors prime cis-regulatory elements required for macrophage and B cell identities. Mol Cell. 2010; 38:576–589. [PubMed: 20513432]

75. Bailey TL, et al. MEME SUITE: tools for motif discovery and searching. Nucleic Acids Res. 2009; 37:W202–W208. [PubMed: 19458158]

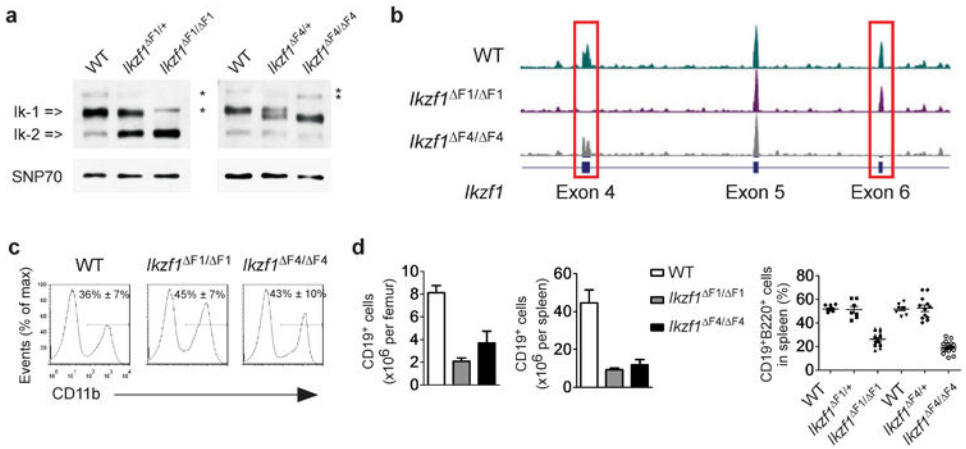

Figure 1.

Adult B cells are present in mice with germline deletion of *Ikzf1* exons encoding zinc fingers 1 or 4. (**a**) Immunoblot analyses with thymocyte extracts from the *Ikzf1*$^{\Delta F1/\Delta F1}$ strain and the *Ikzf1*$^{\Delta F4/\Delta F4}$ strain. The bands denoted with an asterisk correspond to an unidentified form of Ikaros, most likely a post-transcriptionally modified form of Ik-1 (and Ik-2 after exon 4 deletion). SNP70 is shown as a loading control (bottom). (**b**) RNA-Seq analyses of thymocyte mRNAs (n = 4) confirmed the absence of reads from exons 4 and 6 in the *Ikzf1*$^{\Delta F1/\Delta F1}$ and *Ikzf1*$^{\Delta F4/\Delta F4}$ strains, respectively. (**c**) CD11b^{+} myeloid-cell percentages analyzed in bone marrow from 6-week-old wild-type and mutant mice. One experiment is shown with average ± SEM for wild-type (WT) (n = 21), *Ikzf1*$^{\Delta F1/\Delta F1}$ (n = 10) and *Ikzf1*$^{\Delta F4/\Delta F4}$ (n = 14) strains. (**d**) CD19^{+} (left) and CD19^{+}B220^{+} (right) B lineage cells analyzed in the bone marrow (BM) and spleen of 6-week-old mice from the two mutant strains. Average cell numbers ± SEM (left and middle) and % of live cells (right, horizontal bar represents the mean) from wild-type (n = 12–20), *Ikzf1*$^{\Delta F1/\Delta F1}$ (n = 9–18) and *Ikzf1*$^{\Delta F4/\Delta F4}$ (n = 6–17) mice are shown.

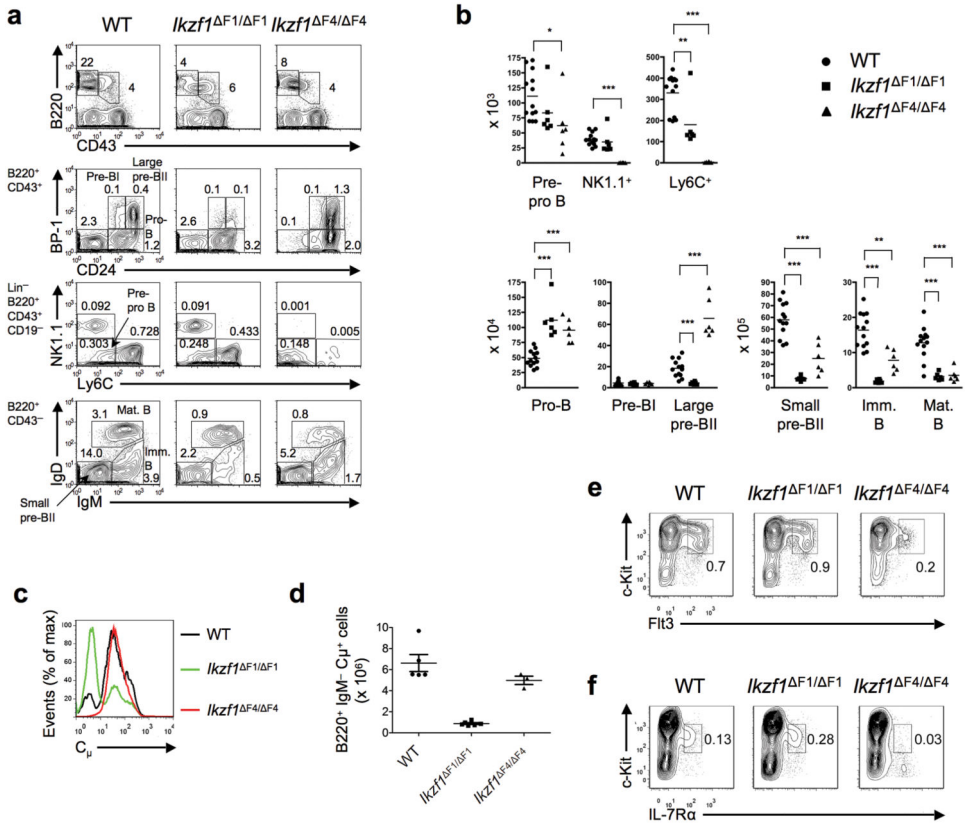

Figure 2.

B cell development is disrupted at different stages in *Ikzf1*$^{\Delta F1/\Delta F1}$ and *Ikzf1*$^{\Delta F4/\Delta F4}$ mice. (**a**). B-cell development was analyzed in whole bone marrow from 6- to 8-week-old mice. One representative experiment out of three or more is shown. Staining is shown for total bone marrow in row 1, pre-pro B to large pre-BII (B220^{+}CD43^{+}) cells in row 2, lineage (Lin)$^{-}$ B220^{+}CD43^{+}CD19^{-}cells (for analysis of pre-pro B) in row 3, and small pre-BII to mature B (B220^{+}CD43^{-}) cells in row 4. The average percentage of the indicated population in total bone marrow is shown. Lineage markers included CD3, TER119, Gr-1, and CD11b. (**b**) Absolute numbers of the indicated populations in total bone marrow of wild-type (n=13), *Ikzf1*$^{\Delta F1/\Delta F1}$ (n=6) and *Ikzf1*$^{\Delta F4/\Delta F4}$ (n=6-8) mice are shown. Each symbol represents an individual mouse and bar shows the mean. **P*<0.05, ***P*<0.01, ****P*<0.001. (**c**) Cytoplasmic Ig μ expression was analyzed in bone marrow cells, gated on B220^{+}IgM^{-}. One representative out of four separate experiments is shown (**d**) Absolute numbers of B220^{+}IgM^{-}cμ^{+} cells per femur are shown. Each symbol represents an individual mouse and bar shows the mean ± SEM of wild-type (n=5), *Ikzf1*$^{\Delta F1/\Delta F1}$ (n=6) and *Ikzf1*$^{\Delta F4/\Delta F4}$ (n=3) mice. (**e-f**) Flt3 and IL-7Rα expression was analyzed on c-Kit^{+} bone marrow cells gated on Lin$^{neg–lo}$ cells. One representative experiment is shown with the average percentage of total live bone marrow cells from wild-type (n=12-14), *Ikzf1*$^{\Delta F1/\Delta F1}$ (n=3-4) and *Ikzf1*$^{\Delta F4/\Delta F4}$ (n=8-9) mice.

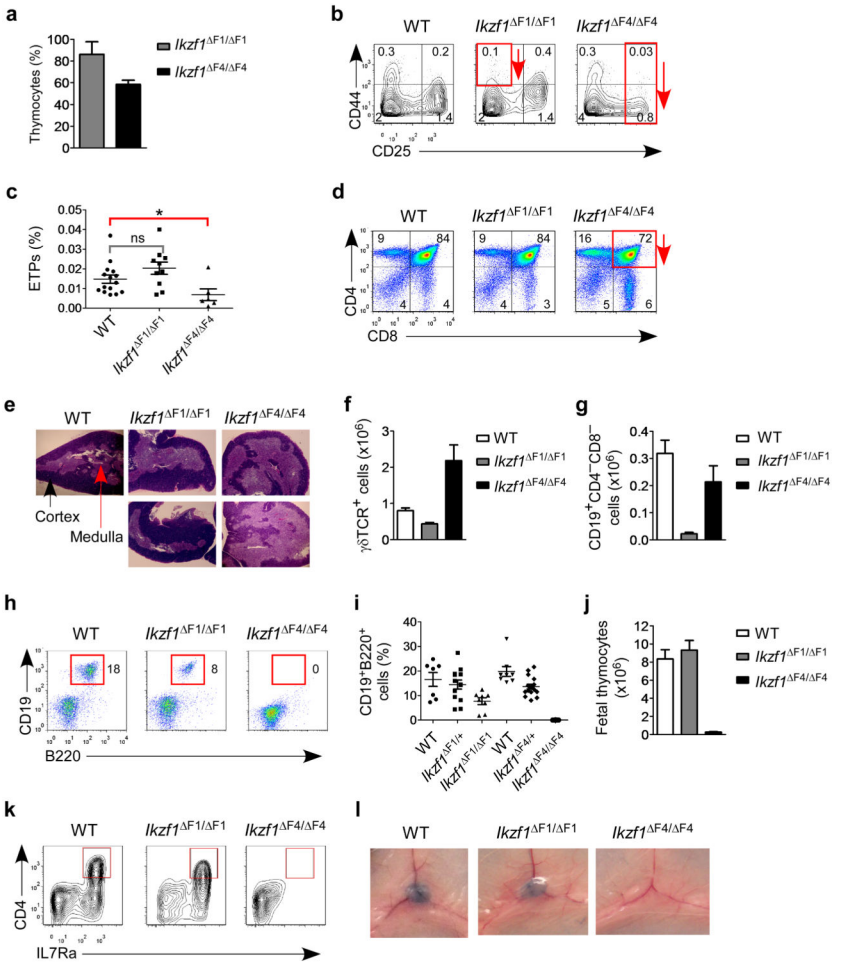

Figure 3.

Selective thymocyte and fetal phenotypes in *Ikzf1*$^{\Delta F1/\Delta F1}$ and *Ikzf1*$^{\Delta F4/\Delta F4}$ mice. Thymocyte development was analyzed with 4-week-old mice, while fetal hematopoietic development was analyzed with E18.5 liver, mesentery, and thymus. (**a**) Thymic cellularity is shown relative to wild-type littermate controls for *Ikzf1*$^{\Delta F1/\Delta F1}$ (n=8) and *Ikzf1*$^{\Delta F4/\Delta F4}$ (n=9) mice. (**b**) Early stages of thymocyte development were analyzed gated on CD4^{-}CD8^{-} (DN) cells. Numbers in quadrants indicate average percentages of CD44^{+}CD25^{-} (DN1), CD44^{+}CD25^{+} (DN2), CD44^{-}CD25^{+} (DN3) and CD44^{-}CD25^{-} (DN4) cells. (**c**) The ETP population (Lin^{-}Kit^{+}CD44^{+}CD25^{-}) were analyzed in wild-type, *Ikzf1*$^{\Delta F1/\Delta F1}$ (n=11), and *Ikzf1*$^{\Delta F4/\Delta F4}$ mice (n=11). *P<0.05 (**d**) Analysis of CD4 and CD8 expression in the thymus. In **b** and **d**, one representative experiment is shown with average values for the indicated populations for wild-type (n=16), *Ikzf1*$^{\Delta F1/\Delta F1}$ (n=8) and *Ikzf1*$^{\Delta F4/\Delta F4}$ (n=8) mice. (**e**) Histological analysis with H&E staining of thymi from 4-week-old mice. (**f-g**) Thymic γδTCR^{+} cells and thymic B cells (CD19^{+}CD4^{-}CD8^{-}) were analyzed in *Ikzf1*$^{\Delta F1/\Delta F1}$ mice (n=8-9) and *Ikzf1*$^{\Delta F4/\Delta F4}$ mice (n=8-11). (**h-i**) Fetal (E18.5) B cells (CD45^{+}CD19^{+}B220^{+}) were analyzed in the *Ikzf1*$^{\Delta F1/\Delta F1}$ strain (n=8) and the *Ikzf1*$^{\Delta F4/\Delta F4}$ strain (n=9). (**j**) The number of fetal thymocytes was selectively reduced in E18.5 *Ikzf1*$^{\Delta F4/\Delta F4}$ embryos (n=10). (**k**) Lymphoid tissue inducer cells (LTi, CD45^{+}CD3e^{-}CD4^{+}IL-7Ra^{+}) were selectively absent in the fetal

mesentery of the *Ikzf1*$^{\Delta F4/\Delta F4}$ strain. (**l**) Inguinal lymph nodes and other peripheral lymph nodes (not shown) were selectively absent in adult *Ikzf1*$^{\Delta F4/\Delta F4}$ mice, as visualized with Evan's Blue. One representative of two or more experiments are shown (**k,l**)

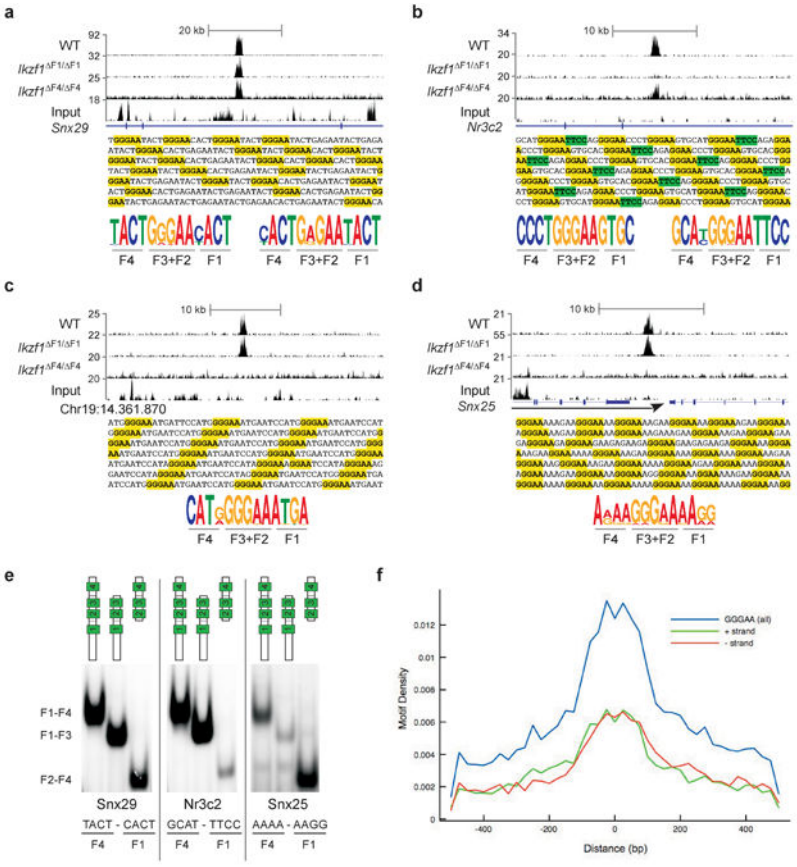

Figure 4.

Differential DNA binding of Ikaros in *Ikzf1*$^{\Delta F1/\Delta F1}$ and *Ikzf1*$^{\Delta F4/\Delta F4}$ thymocytes. (**a-d**) Ikaros ChIP-Seq was performed with thymocytes from 4-week-old wild-type and mutant mice. UCSC genome browser tracks are shown for four genomic regions that contain repetitive Ikaros recognition motifs, thereby yielding unusually strong ChIP-Seq peaks. Examples of interactions that do not depend on neither finger 1 nor finger 4 (*Snx29*), that depend on finger 1 (*Nr3c2*), or that depend on finger 4 (Chr19 and *Snx25*) are shown. Input genomic DNA was sequenced as a negative control. The repetitive genomic sequences are shown below the tracks, with putative Ikaros recognition sites in yellow (GGGAA or GGAA) and green (TTCC). Position weight matrices of the putative Ikaros recognition sequences that were repeated are shown at the bottom, with the zinc fingers predicted to contact or lie in close proximity to the nucleotides indicated (F1-F4). (**e**) Electrophoretic mobility shift assays were performed with oligonucleotide probes from three repetitive sequences and recombinant proteins containing Ikaros fingers 1-4, 1-3, or 2-4. Zinc fingers predicted to contact or lie in close proximity to the nucleotides flanking the GGGAA core recognition sequence are indicated at the bottom (F1 or F4). (**f**) Bioinformatics analysis of a wild-type Ikaros ChIP-Seq dataset revealed the localization of the core GGGAA sequence relative to the center of each ChIP-Seq peak.

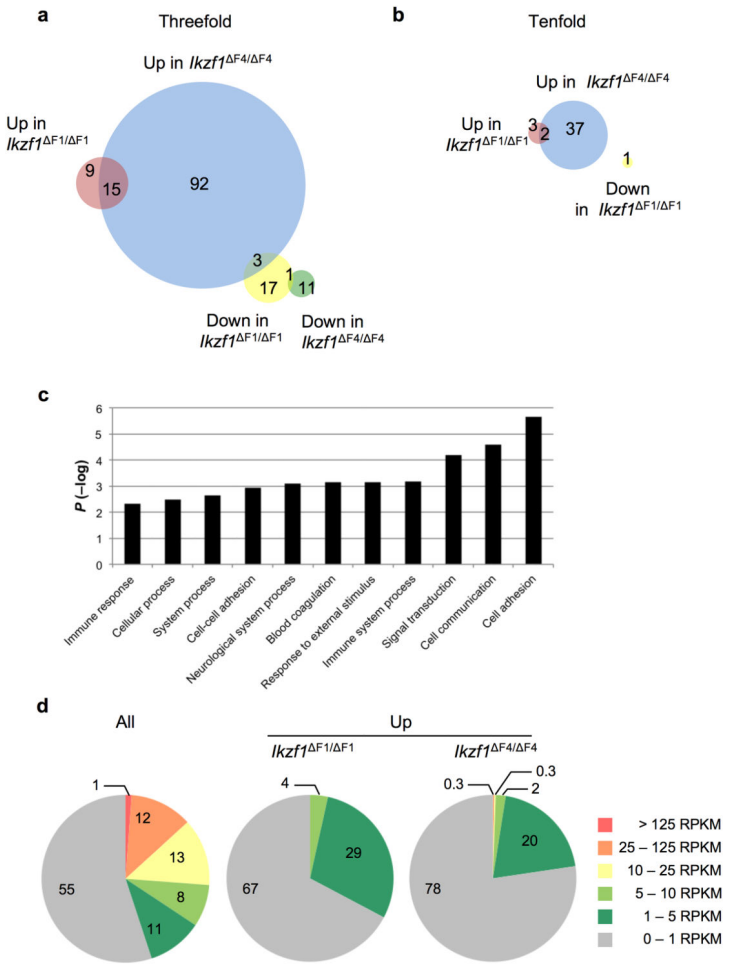

Figure 5.

Deregulation of distinct sets of genes in *Ikzf1*$^{\Delta F1/\Delta F1}$ and *Ikzf1*$^{\Delta F4/\Delta F4}$ DP thymocytes. (**a**) RNA-Seq was performed with FACS-sorted DP thymocyte mRNA from 4-week-old wild-type and mutant mice in duplicate. A Venn diagram shows the number of genes that exhibited increased or decreased mRNA levels of at least 3-fold ($P \leq 0.001$) in one of the mutant strains. Genes with RPKM≥4 in at least one of the six samples were included in this analysis. (**b**) A Venn diagram shows the number of genes from the RNA-Seq experiment described above that exhibited increased or decreased mRNA levels of at least 10-fold ($P \leq 0.001$) in one of the mutant strains. (**c**) Gene Ontology analysis of genes upregulated more than 3-fold ($P \leq 0.001$) in *Ikzf1*$^{\Delta F4/\Delta F4}$ DP thymocytes. (**d**) The distribution of RPKMs (mRNA levels) is shown for all annotated genes (left) and all genes that were upregulated by at least 3-fold ($P \leq 0.001$) in *Ikzf1*$^{\Delta F1/\Delta F1}$ (middle) or *Ikzf1*$^{\Delta F1/\Delta F1}$ (right) mutant mice.

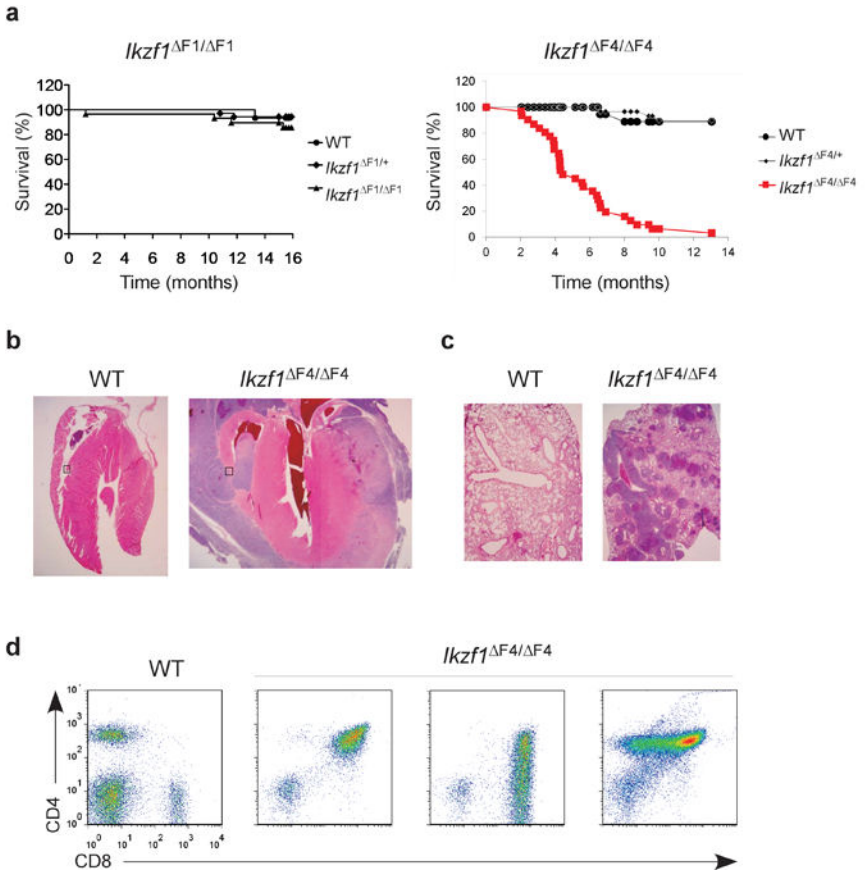

Figure 6.

Ikzf1$^{\Delta F4/\Delta F4}$ but not *Ikzf1*$^{\Delta F1/\Delta F1}$ mice develop spontaneous thymic lymphoma. (**a**) Kaplan-Meier survival curves reveal premature death of *Ikzf1*$^{\Delta F4/\Delta F4}$ mice due to thymic lymphoma. (**b**) Histochemical analysis with H&E stain of an *Ikzf1*$^{\Delta F4/\Delta F4}$ mouse where the thymic lymphoma engulfed the heart (right panel) (n=3). A wild-type control is also shown (left panel). (**c**) Histochemical analysis with H&E stain of an *Ikzf1*$^{\Delta F4/\Delta F4}$ mouse (right panel) revealed thymic lymphoma infiltrating the lung. (**d**) Variable CD4 and CD8 expression was observed in lymphomas that had metastasized to the spleen in three representative *Ikzf1*$^{\Delta F4/\Delta F4}$ mice. Wild-type spleen cells are shown as a control. Figures **c-d** display one representative for each of six or more sick mice analyzed.

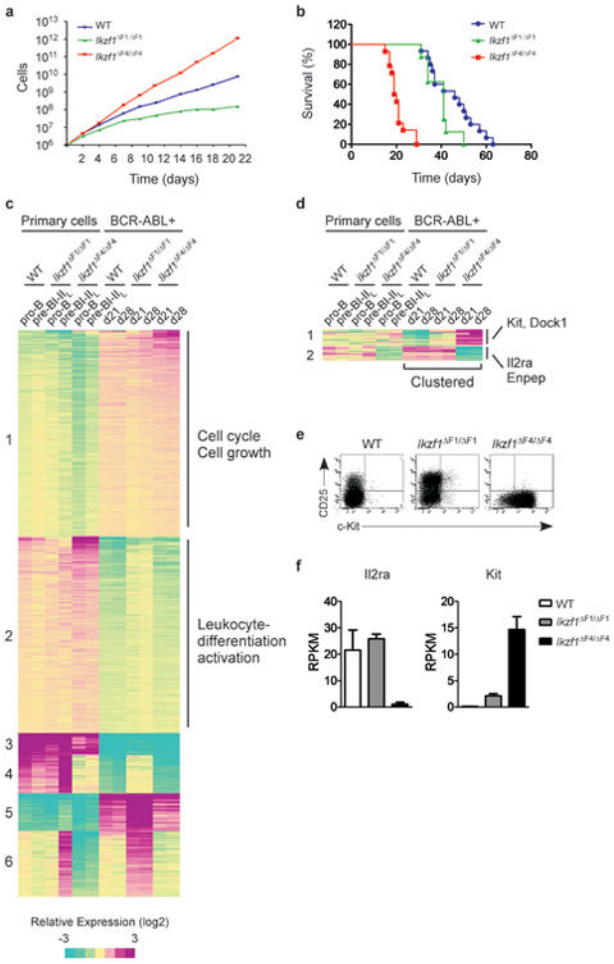

Figure 7.

Selective synergy between BCR-ABL and the *Ikzf1*$^{\Delta F4/\Delta F4}$ mutation *in vitro* and *in vivo*. (**a**) *In vitro* growth curves from one representative experiment (of three) are shown for bone marrow cells from wild-type, *Ikzf1*$^{\Delta F1/\Delta F1}$, and *Ikzf1*$^{\Delta F4/\Delta F4}$ mice transduced with a BCR-ABL-expressing retrovirus and grown under B-ALL culture conditions. (**b**) Kaplan-Meier survival curves are shown for irradiated recipient mice transplanted with 10^6 BCR-ABL-transduced bone marrow cells from wild-type (n=15), *Ikzf1*$^{\Delta F1/\Delta F1}$ (n-8), and *Ikzf1*$^{\Delta F4/\Delta F4}$ (n=14) mice. (**c**) RNA-Seq was performed with mRNA from sorted pro B cells (pro-B) and pre-BI+large pre-BII cells (pre-BI-II$_L$), as well as from BCR-ABL-transformed wild-type, *Ikzf1*$^{\Delta F1/\Delta F1}$, and *Ikzf1*$^{\Delta F4/\Delta F4}$ cells harvested at day 21 (d21) or day 28 (d28) in culture. Genes whose mRNA levels differed by 3-fold or more between any two samples among the 12 samples analyzed were clustered by k-means clustering. (**d**) Genes that were selectively upregulated or downregulated in BCR-ABL-transformed *Ikzf1*$^{\Delta F4/\Delta F4}$ cells were identified by k-means clustering of the data sets from the six BCR-ABL-transformed cultures. Only the two clusters containing genes that were selectively upregulated or downregulated in the *Ikzf1*$^{\Delta F4/\Delta F4}$ samples are shown. Expression data from pro B cells (pro-B) and pre-BI+large pre-BII cells (pre-BI-II$_L$) were aligned after the cluster analysis was completed. (**e**) One representative flow cytometry experiment out of three or more is shown for the *in vitro*

cultures described in panel **a**. Cells are gated on YFP^+ cells. (**f**) Reduced *Il2ra* (CD25) and increased *Kit* mRNA levels are shown from the RNA-seq data (n=2).